2023 10th IEEE International Conference on Power Systems (ICPS)
13-15 December 2023, Cox's Bazar, Bangladesh

Autonomous Power Management and Control Among Interconnected Standalone Hybrid Microgrids

Moshammed Nishat Tasnim[1], Tofael Ahmed[2], Shameem Ahmad[3], and Saad Mekhilef[4]
[1,2]*Advanced Power System Laboratory, Department of Electrical & Electronic Engineering, Chittagong University of Engineering and Technology (CUET), Chittagong 4349, Bangladesh*
[3]*Department of Electrical & Electronic Engineering, Faculty of Engineering, American International University - Bangladesh (AIUB), Dhaka 1229, Bangladesh*
[4]*Distinguished Professor, Swinburne University of Technology, Hawthorn, Melbourne, Victoria 3122, Australia*
Email- mnishattasnim1@gmail.com, tofael@cuet.ac.bd, ahmad.shameem@aiub.edu, smekhilef@swin.edu.au

***Abstract*— Multiple microgrids (MGs) being interconnected permits a high penetration of renewable energy sources while also improving the reliability and generation efficiency of the interconnected MG system. However, an effective power management strategy (PMS) and reliable control structure are required to ensure suitable operation and proper power sharing. Therefore, an effective clustering method of three hybrid MGs with a decentralized control structure is proposed in this paper to ensure sufficient power supply in three MGs depending on their available power generation in islanded mode. The interconnection takes place among the DC buses of each hybrid MG using a bidirectional DC/DC converter, which eliminates the complexity of reactive power management and synchronization and reduces power losses and costs. Moreover, the proposed decentralized PMS is based on the system voltage deviation to achieve proper power sharing without any communication link. Different scenarios for power sharing among interconnected hybrid MGs, including load variations, source failure, and energy storage systems charging or discharging, are analyzed. The performance of the proposed interconnection method and PMS is analyzed and validated using MATLAB/Simulink and a real-time-based OPAL-RT digital simulator. The simulation outcomes show that the proposed method and PMS ensure reliable operation and provide proper power sharing among the three hybrid MGs.**

Keywords*— *Hybrid microgrid, DC/DC converter, interconnected microgrids, islanded mode, power sharing

I. INTRODUCTION

The microgrid (MG) is a type of electrical network that can effectively integrate distributed energy resources (DERs), energy storage systems (ESSs), utility grids, and loads that may function in both islanded mode and grid-connected mode [1]. In recent years, these renewable energy sources (RESs)-based MG systems have gained popularity as a way to meet the growing energy demand while also addressing difficulties such as losses in long transmission lines, diminishing fossil fuel resources, and environmental concerns [2]. However, a single MG can only produce and distribute power within a specific area, and the intermittent nature of RES units results in fluctuations in output power, voltage, and frequency. Moreover, due to the constrained generation capability during the islanded mode, the single MG cannot guarantee the security of the load requirement. As a result, it will use load-shedding techniques to maintain demand when one or more DER units are unavailable or fail. Therefore, the interconnected MG (IMG) system has evolved into a flexible, integrated framework that includes numerous distinct MGs that are adjacent to one another [3]. The IMG system's primary features involve promoting efficient management of energy consumption as well as high utilization and effective sharing of DERs. IMGs, whether in the grid-connected mode or the islanded mode, exhibit favorable economic traits. In IMGs, power sharing across the MGs enables the MGs to meet their power needs with their own less expensive RESs and lowers the energy losses associated with long-distance transmissions. Moreover, the IMGs in the distribution network will significantly increase the application of RESs and lessen the load on the main grid by facilitating energy exchanges, alleviating overstress on distribution lines, and enhancing their own and the main grid's reliability [4].

DC interlinking devices and DC/DC converters are used to interconnect DC IMGs; AC interlinking devices and AC/AC converters are used to interconnect AC IMGs; and mixed DC and AC MGs are interconnected through DC/AC converters. In [5], a comprehensive model and small-signal analysis for photovoltaic (PV)-based MG clusters are developed, considering the local adaptive dynamic droop control structure of the voltage-source PV system. To design high-level controllers, such as inter-MG energy trading controllers, for large-scale interconnected AC MGs that are interconnected by interlinking lines, a low-frequency and small-signal model is proposed in [6]. A distributed control strategy with primary, secondary, and tertiary levels is proposed in [7] to regulate power sharing among a group of DC MGs. Whereas primary and secondary controllers control power sharing among the sources in a single DC MG, tertiary controllers are necessary to provide higher-level power sharing among MGs. In order to regulate DC-bus voltages in DC MGs with ZIP (constant impedance, constant current, and constant power) loads and achieve proportional power sharing, a consensus-based technique is provided in [8]. However, a more flexible operation in terms of voltage, frequency, and power controls can be accomplished with the use of converter interfaces, even though interconnecting MG clusters with interlinking lines is simpler [9]. In [10], a network of MG clusters is constructed by interconnecting several MGs through an inverter, where each MG consists of DER units and ESSs and operates in islanded mode. Future MG implementation will be facilitated

979-8-3503-1873-9/23/$31.00 ©2023 IEEE

by hybrid MGs, which connect AC and DC MGs. In [11], a three-phase back-to-back active power converter for MG clusters is suggested using a DC-link voltage-controlling approach. In order to achieve high stability, the converter's required active and reactive power can help control the frequency and voltage of MGs. The back-to-back converter's DC-link capacitor is also essential for power decoupling and power balancing. In [12], numerous interlinking techniques, control challenges with AC and DC MGs, and finally, various interlinking converter control strategies are comprehensively discussed. The frequency of each AC MG is different in the stand-alone IMG system proposed in [13], and a back-to-back converter is used to connect the nearby MGs. By creating a suitable controller for the back-to-back converter, the IMG system's frequency performance can be enhanced.

However, researchers are becoming increasingly interested in interconnection utilizing DC buses because of their benefits in reducing control complexity, synchronization, reactive power, and harmonics. Additionally, DC MGs have many advantages over AC MGs, including no frequency synchronization, no reactive power management, simplicity of the control topology, dependability, and efficiency. The planning, operation, stability, and control of DC MGs are the subject of several studies. In [14], a comparative evaluation of recent studies on the management of DC MG clusters is proposed. In order to perform voltage management and power sharing, a cascaded control structure is suggested in [15]. In [16], a networking method for two MGs using a static switch with a proper power sharing approach is proposed to ensure power supply in both MGs. However, interconnection using a converter interface provides more flexible operation in terms of voltage and frequency control and power sharing [17]. Moreover, all the above-mentioned studies did not provide a good insight into the interconnection of hybrid MGs using DC/DC converters, power sharing, and power balancing, considering ESS's functionality and the power management system (PMS) of the IMG system. Therefore, to address these issues, this study presents a clustering method for three hybrid MGs using a bidirectional DC/DC converter (BDC) and a control structure. The contributions to this paper are given by:

- A clustering method to interconnect three hybrid MGs operating in islanded mode using the converter interface of a BDC is proposed.
- A decentralized control structure is proposed to ensure continuous power supply to all the hybrid MGs during islanded mode.
- The performance of the proposed method is analyzed with a PMS, considering load variations, DER unit failure, and ESS charging and discharging phases.

The paper is organized as follows: Section II describes the configuration of the IMG system. The clustering method using BDC and control structures is also presented in this section. Section III contains the results based on the IMG system's performance analysis under different scenarios. Finally, the conclusion of this study is presented in Section IV.

II. IMG System Configuration

The IMG system structure and the structure of the DC/DC interconnecting converter and controller strategy are presented in this section. The required parameters for the IMG system framework are listed in Table I. In this study, similar DERs have the same rating for better and simpler analysis. The maximum generating capacity of each hybrid MG is 101kW and the overall capacity of the IMG system is 303kW.

TABLE I. IMG System Parameters

Systems	Parameters and Symbols	Values
PV generator	Maximum power at irradiance 1000W/m^2 and tenperature 25°C	41kW
Wind generator	Maximum power at wind speed 15m/s^2	40kW
ESS	Lithium-ion battery	
	Rated Voltage	12V
	No of batteries in series	27
	Rated power	25kW
	SoC	20≤SoC≤80
	Capacity	77Ah
System aspects	RMS AC-bus voltage	220V
	DC-bus voltage, V_{bus}	800V
	Sampling time, T_s	50μs
	System frequency, f	50Hz
	DC-bus Capacitance, C_{bus}	5000μF
	LCL filter	
	Grid-side Inductance, L_2	6mH
	Capacitance, C_f	10μF
	Damping Resistor, R_D	5Ω
	VSC-side Inductance, L_1	0.5mH
BDC	Inductance	10mH
	Capacitance	500μF
	Proportional gain, k	1e-4
	Swithching frequency	3kHz
	PI Controllers	
	Proportional gains, ($k^{dc}{}_{p_V}$, $k^{ac}{}_{p_v}$, k_{p_I})	1, 0.5, 0.5
	Integral gains, ($k^{dc}{}_{i_V}$, $k^{ac}{}_{i_v}$, k_{i_I})	5, 3, 1

A. System Configuration

The configuration shown in Fig. 1 has been employed to analyze the power sharing in an IMG system. The system consists of three hybrid MGs operating in islanded mode. Each hybrid MG consists of PV generators, wind generators, and ESSs. PVs and ESSs are designed as DC sources, and wind generators are designed as AC sources. The generation of PV and wind generators varies according to solar irradiance and wind speed. Therefore, each MG undergoes significant power variations because of the intermittence characteristics of PV and wind generators. Therefore, a backup or dependable power supply is required to meet the load requirements, regardless of the DER's power variation. ESSs are recommended as a reliable power source since they are able to deliver a consistent supply for extended periods of time.

A unidirectional DC/DC boost converter connects the PV array to the DC bus. In order to get the maximum possible power from the PV system, it should be run with maximum power point tracking (MPPT). The perturb and observe algorithm (P&O) has been employed as the MPPT in this study.

A doubly-fed induction generator (DFIG)-based wind generator with a back-to-back converter is used. The back-to-back converter consists of an IGBT-based rotor-side converter and a grid-side converter. Such converters are capable of MPPT, controlling voltage and reactive power, compensating for unbalanced grid conditions, and stabilizing oscillations. The lookup table is used in the rotor-side converter control loops to determine the reference torque and capture the maximum wind power. Reactive power is regulated by the d-axis loop, whereas active power is regulated by the q-axis loop. The d-axis loop controls the terminal voltage, whereas the q-axis loop controls the DC-link voltage in the grid-side converter control loops [18].

In this study, a battery-based ESS is connected to the system DC bus using a BDC. ESSs may be utilized by a distributed generator or individually coupled to a MG. BDC are crucial for connecting ESSs with the MG system, controlling the amount and direction of power in ESSs, and regulating the DC-bus voltage, regardless of the type of MG. When there is excess power in the system, the BDC transmits power to charge the battery, and when DER power is insufficient to meet load demand, the same BDC transfers the battery's stored energy.

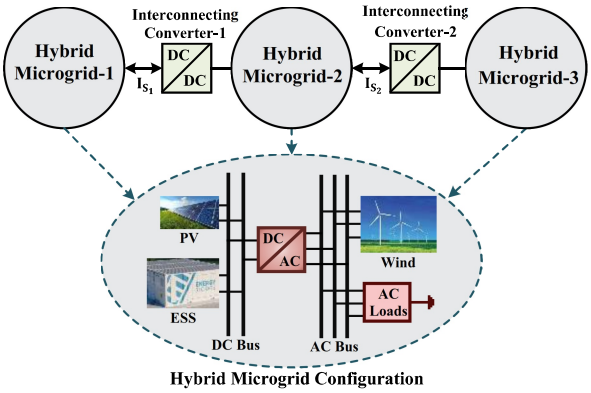

Fig. 1. Configuration of the serial interconnecting MG system using DC/DC converter.

B. *Converter structure and Power Management System*

The interlinking converter of each hybrid MG is controlled based on the active power and frequency (P-f) droop characteristics as given by

$$f_i = f^{ref}{}_i - m_i P_i \quad (1)$$

$$P_i = P_{PV_i} + P_{wind_i} \pm P_{ess_i} \quad (2)$$

Where i indicates the number of hybrid MG, m_i is the droop coefficients, P_i is the active power of the equivalent AC and DC DERs of the individual MG, $f^{ref}{}_i$ is the reference frequency of the individual MG, f_i is the measured frequency, P_{PV_i} is the PV generation, P_{wind_i} is the wind generation, and P_{ess_i} is the charging or discharging power of ESS.

The outer control loop of the interlinking converter is based on an AC voltage controller. PI controllers are used to reduce the error between the reference voltage and their corresponding measured voltage magnitudes. The signals obtained from the inner current controller are used to obtain the switching signals of the voltage source converter (VSC) using the SPWM technique [19].

The configuration of the BDC and its related controller is shown in Fig. 2. A buck converter and a boost converter are combined to create the BDC circuit. This method enables 4-quadrant operation; as a result, this topology operates in both buck mode and boost mode. The most adaptable topology is this one because of its 4-quardant operation. PI controller-based control technique is used, as shown in Fig. 3, in order to avoid control complexity and increase physical flexibility [20]. The outer controller of the BDC consists of a DC voltage, $G_{V_{dc}}(s)$, and an AC voltage controller, $G_{v_{ac}}(s)$, and the inner current controller consists of a current controller, $G_I(s)$. The transfer functions of these controllers are given by,

$$G_{V_{dc}}(s) = k^{dc}{}_{p_V} + \frac{k^{dc}{}_{i_V}}{s} \quad (3)$$

$$G_{v_{ac}}(s) = k^{ac}{}_{p_v} + \frac{k^{ac}{}_{i_v}}{s} \quad (4)$$

$$G_I(s) = k_{p_I} + \frac{k_{i_I}}{s} \quad (5)$$

Where $k^{dc}{}_{p_V}$ and $k^{dc}{}_{i_V}$ are the proportional and integral gains of the DC voltage controller, $k^{ac}{}_{p_v}$, and $k^{ac}{}_{v}$ are the proportional and integral gains of the AC voltage controller, and k_{p_I}, and k_{i_I} are the proportional and integral gains of the current controller.

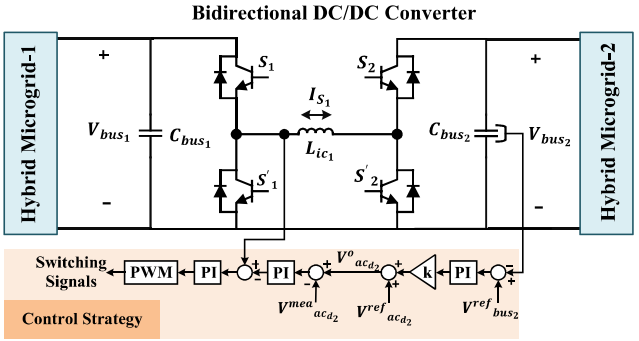

Fig. 2. Configuration of the bidirectional DC/DC interlinking converter and its associated control strategy.

The operation of the proposed IMG system can be categorized into three cases, as shown in Table II, and Fig. 3 illustrates the PMS for the IMG system operation under these cases. This flowchart is designed to represent the power sharing and power balance in the IMG system. If any MG has a net surplus (or deficit) of power, the PMS guarantees that power is exported to (or imported from) the neighboring MGs. This ensures that the voltage and frequency of the whole system are within the prescribed limits and that effective power sharing among the three MGs is allowed. In this system, negative power indicates the discharging operation of all ESSs (SoC decreases), and positive power indicates their charging operation (SoC increases).

TABLE II. OPERATING SCENARIOS OF IMG SYSTEM

Cases	Description
Case I	Nearly zero power sharing among MGs.
Case II	Power sharing from MG-1 to MG-2; MG-2 to MG-3
Case III	Power sharing from MG-3 to MG-2; MG-2 to MG-1

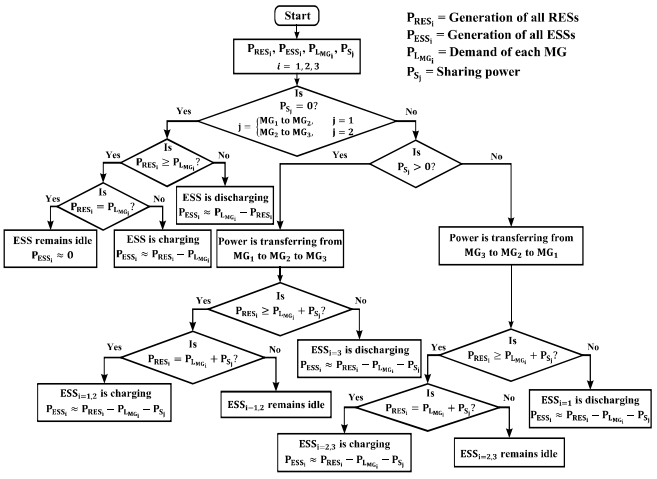

Fig. 3. The flowchart of the power management system.

III. RESULT AND ANALYSIS

The performance of the whole IMG model is verified with a time step of 50μs or a sampling frequency of 20kHz utilizing a real-time simulator called OPAL-RT (OP5600), MATLAB/Simulink, and RT-LAB software, as illustrated in

Fig. 4. The parameters listed in Table I are used to design the whole IMG system. Three power sharing cases, as described in Table II and Fig. 3, have been considered to analyze the performance of the proposed IMG system. A summary of power generation, consumption, and sharing in three cases is presented in Table III.

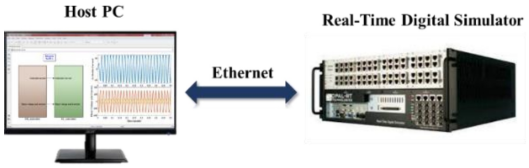

Fig. 4. Real-time software-in-the-loop implementation.

A. Case I

Fig. 5 illustrates the performance of the IMG system in the case of nearly zero power sharing, i.e., when the generation of individual hybrid MGs is sufficient to satisfy load requirements. In this case, a certain load consisting of constant power loads (resistive inductive) and dynamics loads (induction motor) is maintained in all three hybrid MGs, as shown in Fig. 5 (a). The generation of each source in each hybrid MG is illustrated in Figs. 5 (b), (c), and (d). The PV generations are at 33.5kW at 800W/m^2, 38kW at 900W/m^2, and 41kW at 1000W/m^2 irradiance, and the wind generation is 25kW at 11m/s^2 wind speed, as shown in Figs. 5 (b), (c), and (d). The ESS of each hybrid MG is charging at nearly 20kW, as the state-of-charge (SoC) of the ESS is increasing from 70%, as shown in Fig. 5 (e). The sharing of power among the three MGs is 200W, as in each hybrid MG there is sufficient power to fulfill load demand. The system parameters, such as AC voltage at 220V rms, frequency at 50Hz, and DC voltage at 800V, are fixed to their rated limits, as shown in Figs. 5 (g) and (h).

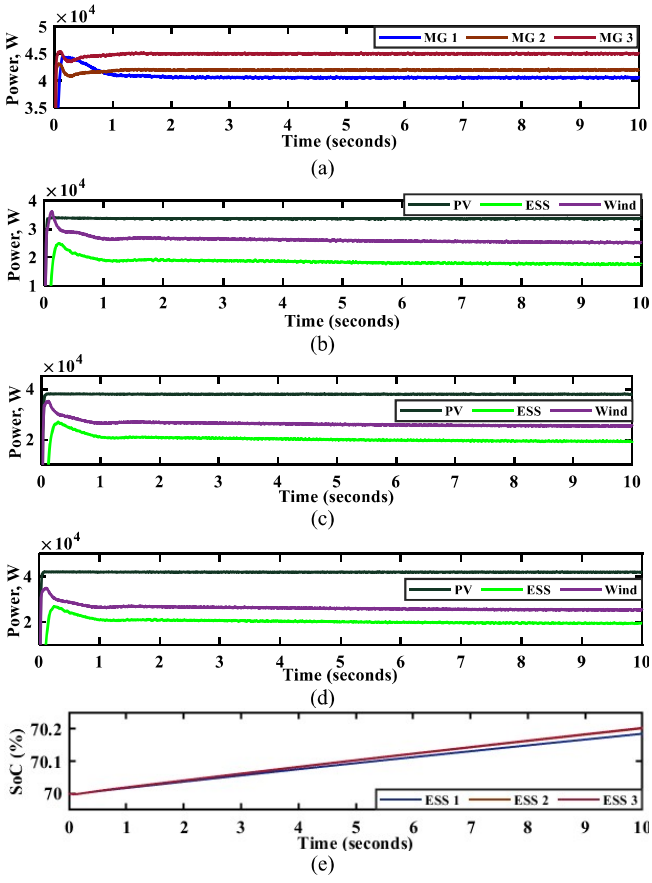

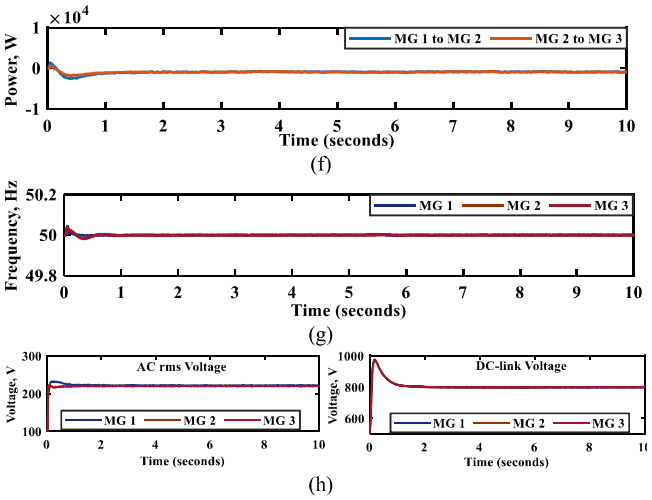

Fig. 5. Simulation results under nearly zero power sharing: a) Load power, b) MG-1 generation, c) MG-2 generation, d) MG-3 generation, e) SoC of the ESS, f) Shared power, g) g) System frequency, i) AC rms voltage and DC-link voltage.

B. Case II

Fig. 6 shows the performance of the IMG system in the case of positive power sharing, i.e., when the power is transferred from hybrid MG-1 to hybrid MG-2 and hybrid MG-2 to hybrid MG-3 to satisfy load requirements and balance power in the system. A 45kW load is maintained in all three hybrid MGs from t = 0 to 1.5s, as shown in Fig. 6 (a). At t = 1.5s, a 30kW load is added in the hybrid MG-3, and at t = 3.5s, a 25kW load is added in the hybrid MG-2. At t = 4.5s, the PV generation in hybrid MG-3 is zero. The sharing of power is positive, i.e., from hybrid MG-1 to hybrid MG-2 and from hybrid MG-2 to hybrid MG-3, in order to balance the power in the entire IMG system. Fig. 6(f) indicates the power sharing curve, and a detailed analysis is presented in Table III. The charging rate of the ESS in each MG decreases, due to which the SoC of the ESSs decreases, as shown in Fig. 6(e). The system parameters at the moment of load changes, such as AC voltage, frequency, and DC voltage, are decreased when load increases and vice versa, as shown in Figs. 6 (g) and (h).

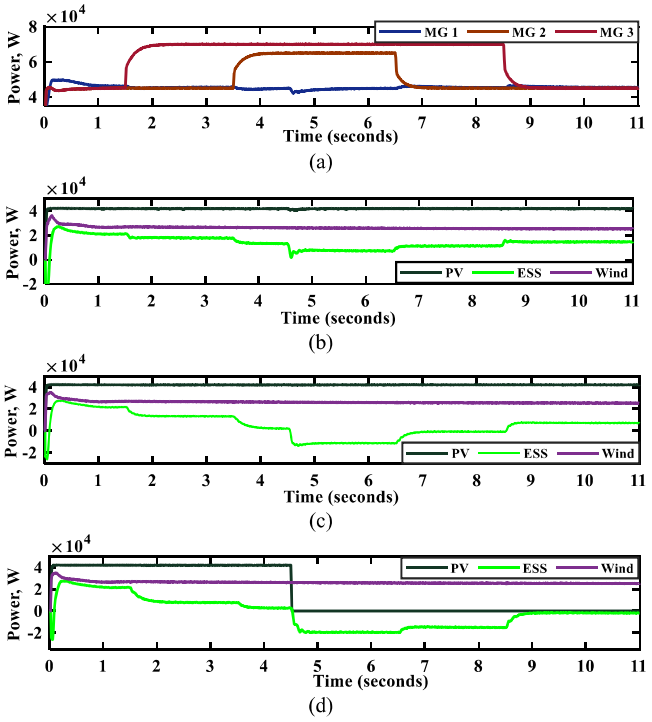

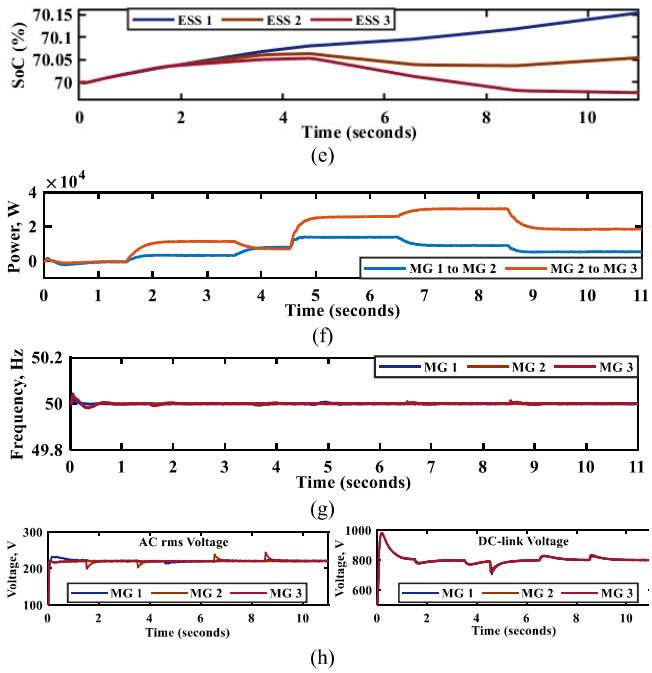

Fig. 6. Simulation results under positive power sharing: a) Load power, b) MG-1 generation, c) MG-2 generation, d) MG-3 generation, e) SoC of the ESS, f) Shared power, g) System frequency, i) AC rms voltage and DC-link voltage.

C. *Case III*

Fig. 7 illustrates the performance of the IMG system in the case of negative power sharing, i.e., when the power is transferred from hybrid MG-3 to hybrid MG-2 and hybrid MG-2 to hybrid MG-1 to satisfy load requirements and balance power in the system. A 45kW load is maintained in three hybrid MGs from t = 0 to 1.5s, as shown in Fig. 7 (a). At t = 1.5s, a 25kW load is added in hybrid MG-1, and at t = 3.5s, a 20kW load is added in hybrid MG-2. The generation of each source in each hybrid MG is considered to have the same rating. The PV generation is fixed at 41kW at 1000W/m^2 irradiance, and the wind generation is 25kW at 11m/s^2 wind speed. At t = 5s, there is another load increment of about 10kW in the hybrid MG-3. The sharing of power is negative in order to balance the power in the entire IMG system. Fig. 7 (f) indicates that 10kW of power is flowing from hybrid MG-2 to hybrid MG-1 and another 5kW from hybrid MG-3 to hybrid MG-1. The charging rate of the ESS in each hybrid MG decreases, due to which the SoC of the ESSs decreases from 70%, as shown in Fig. 7 (e). The system parameters at the moment of load changes, such as AC voltage, frequency, and DC voltage, are slightly decreased when load increases and vice versa, as shown in Figs. 7 (g) and (h).

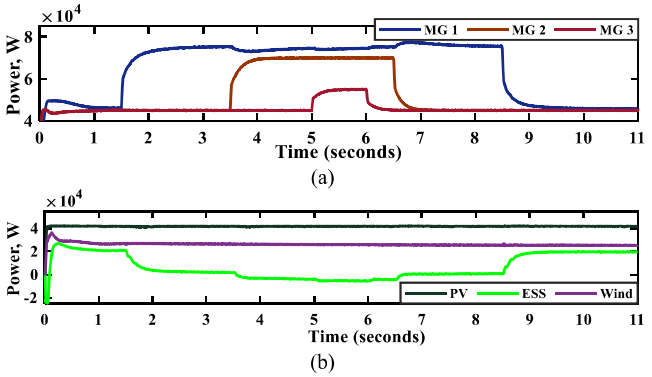

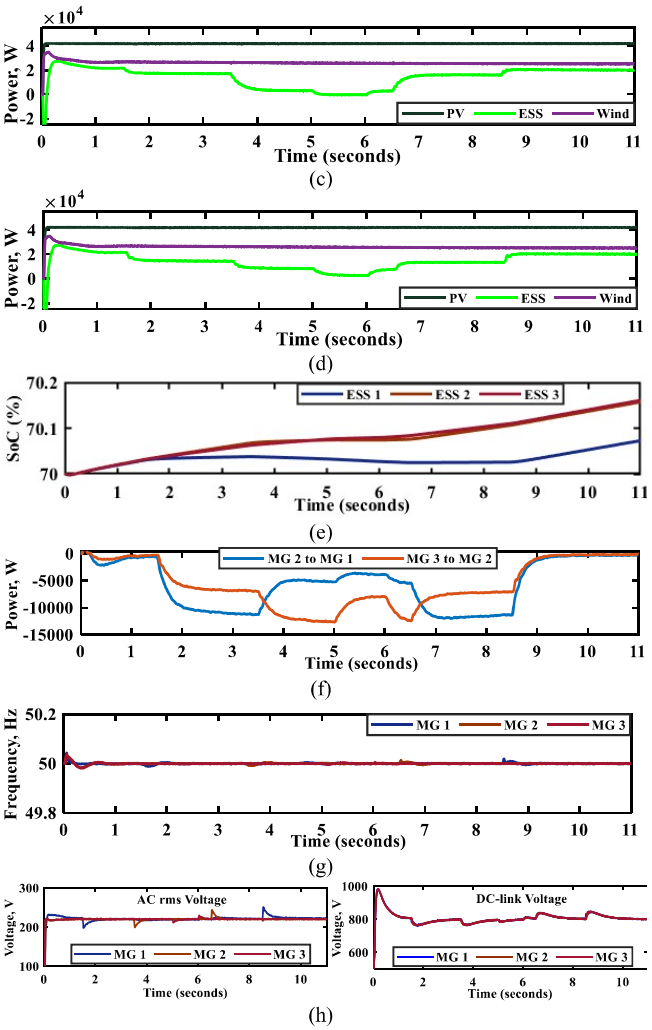

Fig. 7. Simulation results under negative power sharing: a) Load power, b) MG-1 generation, c) MG-2 generation, d) MG-3 generation, e) SoC of the ESS, f) Shared power, g) System frequency, i) AC rms voltage and DC-link voltage.

IV. Conclusion

In this paper, a clustering method and a decentralized control structure for an IMG system are proposed in order to control the power flow among multiple hybrid MGs operating in islanded mode. The most crucial factor is that in the proposed interconnection method, the three hybrid MGs are connected to each other using a BDC instead of a direct tie-line connection. The proposed control structure for the DC/DC converter and decentralized PMS of the IMG system provides reliable and flexible interfaces and a framework for interconnecting several hybrid MGs. Also, the interconnection using converter interfaces enables this system to provide more flexible operation in terms of voltage, frequency, and power sharing regulation. This technique is applicable for any number of interconnected hybrid MGs operating in islanded mode. The performance of the proposed method with control strategies is evaluated in MATLAB/Simulink and the OP5600 digital simulator. The results of the system analysis under different conditions, including load variations, ESS functionality, and source failure, demonstrate that the proposed method with PMS ensures proper power sharing among interconnected hybrid MGs. The results also show that the MGs in the system support one another in the event of DER unit failure in individual MGs (PV failure in hybrid MG-2 at t

TABLE III. A SUMMARY OF THE POWER GENERATION AND CONSUMPTION OF THREE HYBRID MGS

Cases	Time (s)	Hybrid MG -1				Hybrid MG-2				Hybrid MG-3				Sharing
		DERs		ESS	Load	DERs		ESS	Load	DERs		ESS	Load	
		PV	Wind			PV	Wind			PV	Wind			
Case I	0 – 10	33.5 kW (800W/m^2)	25 kW	19 kW	40 kW	38 kW (900W/m^2)	25 kW	19.9 kW	42 kW	41 kW (1000W/m^2)	25 kW	22.6 kW	45 kW	MG 2 to MG 1 – (- 0.5 kW) MG 3 to MG 2 – (- 0.6 kW)
Case II	0 – 1.5	41 kW (1000W/m^2)	25 kW	20.8 kW	45 kW	41 kW (1000W/m^2)	25 kW	21 kW	45 kW	41 kW (1000W/m^2)	25 kW	21.2 kW	45 kW	MG 2 to MG 1 – (- 0.2 kW) MG 3 to MG 2 – (- 0.2 kW)
	1.5 – 3.5	41 kW (1000W/m^2)	25 kW	18 kW	45 kW	41 kW (1000W/m^2)	25 kW	12.5 kW	45 kW	41 kW (1000W/m^2)	25 kW	7.5 kW	70 kW	MG 1 to MG 2 – (3 kW) MG 2 to MG 3 – (11.5 kW)
	3.5 – 4.5	41 kW (1000W/m^2)	25 kW	13 kW	45 kW	41 kW (1000W/m^2)	25 kW	2 kW	65 kW	41 kW (1000W/m^2)	25 kW	3 kW	70 kW	MG 1 to MG 2 – (8 kW) MG 2 to MG 3 – (7 kW)
	4.5 – 6.5	41 kW (1000W/m^2)	25 kW	7 kW	45 kW	41 kW (1000W/m^2)	25 kW	-11 kW	65 kW	0 kW (0W/m^2)	25 kW	-19 kW	70 kW	MG 1 to MG 2 – (14 kW) MG 2 to MG 3 – (26 kW)
	6.5 – 8.5	41 kW (1000W/m^2)	25 kW	11.5 kW	45 kW	41 kW (1000W/m^2)	25 kW	-9 kW	45 kW	0 kW (0W/m^2)	25 kW	-15 kW	70 kW	MG 1 to MG 2 – (9.5 kW) MG 2 to MG 3 – (30 kW)
	8.5 – 11	41 kW (1000W/m^2)	25 kW	15.5	45 kW	41 kW (1000W/m^2)	25 kW	8 kW	45 kW	0 kW (0W/m^2)	25 kW	-1.5 kW	45 kW	MG 1 to MG 2 – (5.5 kW) MG 2 to MG 3 – (18.5 kW)
Case III	0 – 1.5 8.5 – 11	41 kW (1000W/m^2)	25 kW	20.8 kW	45 kW	41 kW (1000W/m^2)	25 kW	21 kW	45 kW	41 kW (1000W/m^2)	25 kW	21.2 kW	45 kW	MG 2 to MG 1 – (- 0.2 kW) MG 3 to MG 2 – (- 0.2 kW)
	1.5 – 3.5	41 kW (1000W/m^2)	25 kW	2 kW	75 kW	41 kW (1000W/m^2)	25 kW	17 kW	45	41 kW (1000W/m^2)	25 kW	14 kW	45 kW	MG 2 to MG 1 – (- 11 kW) MG 3 to MG 2 – (- 7 kW)
	3.5 – 5	41 kW (1000W/m^2)	25 kW	- 4 kW	75 kW	41 kW (1000W/m^2)	25 kW	3.5 kW	70 kW	41 kW (1000W/m^2)	25 kW	8.5 kW	45 kW	MG 2 to MG 1 – (- 5 kW) MG 3 to MG 2 – (- 12.5 kW)
	5 – 6	41 kW (1000W/m^2)	25 kW	- 5.5 kW	75 kW	41 kW (1000W/m^2)	25 kW	- 0.2 kW	70 kW	41 kW (1000W/m^2)	25 kW	2.5 kW	55 kW	MG 2 to MG 1 – (- 4 kW) MG 3 to MG 2 – (- 8 kW)
	6 – 6.5	41 kW (1000W/m^2)	25 kW	- 4 kW	75 kW	41 kW (1000W/m^2)	25 kW	3 kW	70 kW	41 kW (1000W/m^2)	25 kW	9 kW	45 kW	MG 2 to MG 1 – (- 5 kW) MG 3 to MG 2 – (- 12 kW)
	6.5 – 8.5	41 kW (1000W/m^2)	25 kW	1.5 kW	75 kW	41 kW (1000W/m^2)	25 kW	17.5 kW	45 kW	41 kW (1000W/m^2)	25 kW	14 kW	45 kW	MG 2 to MG 1 – (- 10.5 kW) MG 3 to MG 2 – (- 7 kW)

= 4.5s) and minimize the need for unnecessary load shedding techniques to balance supply and demand.

ACKNOWLEDGMENT

The authors thank the Chittagong University of Engineering and Technology (CUET) for providing financial support under the Development of CUET Project and Project No. CUET/DRE/2021-22/EEE/016.

REFERENCES

[1] R. G. Allwyn, A. Al-Hinai, and V. Margaret, "A comprehensive review on energy management strategy of microgrids," *Energy Reports,* vol. 9, pp. 5565-5591, 2023.

[2] M. N. Tasnim, T. Ahmed, S. Ahmad, and S. Mekhilef, "Hardware in The Loop Implementation of The Control Strategies for The AC-Microgrid in OPAL-RT Simulator," in *2023 IEEE IAS Global Conference on Renewable Energy and Hydrogen Technologies (GlobConHT)*, 2023, pp. 1-6: IEEE.

[3] P. Sharma, H. D. Mathur, P. Mishra, and R. C. Bansal, "A critical and comparative review of energy management strategies for microgrids," *Applied Energy,* vol. 327, p. 120028, 2022.

[4] A. Nawaz, M. Zhou, J. Wu, and C. Long, "A comprehensive review on energy management, demand response, and coordination schemes utilization in multi-microgrids network," *Applied Energy,* vol. 323, p. 119596, 2022.

[5] Z. Zhao, P. Yang, Y. Wang, Z. Xu, and J. M. Guerrero, "Dynamic characteristics analysis and stabilization of PV-based multiple microgrid clusters," *IEEE Transactions on Smart grid,* vol. 10, no. 1, pp. 805-818, 2017.

[6] M. Naderi, Q. Shafiee, H. Bevrani, and F. Blaabjerg, "Low-frequency small-signal modeling of interconnected AC microgrids," *IEEE Transactions on Power Systems,* vol. 36, no. 4, pp. 2786-2797, 2020.

[7] S. Moayedi and A. Davoudi, "Distributed tertiary control of DC microgrid clusters," *IEEE Transactions on Power Electronics,* vol. 31, no. 2, pp. 1717-1733, 2015.

[8] B. Fan, S. Guo, J. Peng, Q. Yang, W. Liu, and L. Liu, "A consensus-based algorithm for power sharing and voltage regulation in DC microgrids," *IEEE Transactions on Industrial Informatics,* vol. 16, no. 6, pp. 3987-3996, 2019.

[9] M. J. Hossain, M. A. Mahmud, F. Milano, S. Bacha, and A. Hably, "Design of robust distributed control for interconnected microgrids," *IEEE Transactions on Smart Grid,* vol. 7, no. 6, pp. 2724-2735, 2015.

[10] K. Koyanagi, Y. Hida, R. Yokoyama, S. Nagata, K. Nakao, and T. Hirai, "Electricity cluster-oriented network: A grid-independent and autonomous aggregation of micro-grids," in *2010 Modern Electric Power Systems*, 2010, pp. 1-6: IEEE.

[11] C.-Y. Tang, Y.-F. Chen, Y.-M. Chen, and Y.-R. Chang, "DC-link voltage control strategy for three-phase back-to-back active power conditioners," *IEEE Transactions on Industrial Electronics,* vol. 62, no. 10, pp. 6306-6316, 2015.

[12] M. Zolfaghari, G. B. Gharehpetian, M. Shafie-khah, and J. P. Catalão, "Comprehensive review on the strategies for controlling the interconnection of AC and DC microgrids," *International Journal of Electrical Power & Energy Systems,* vol. 136, p. 107742, 2022.

[13] H.-J. Yoo, T.-T. Nguyen, and H.-M. Kim, "Multi-frequency control in a stand-alone multi-microgrid system using a back-to-back converter," *Energies,* vol. 10, no. 6, p. 822, 2017.

[14] Z. H. A. Al-Tameemi, T. T. Lie, G. Foo, and F. Blaabjerg, "Control strategies of DC microgrids cluster: A comprehensive review," *Energies,* vol. 14, no. 22, p. 7569, 2021.

[15] J. Zhou, M. Shi, X. Chen, Y. Chen, J. Wen, and H. He, "A cascaded distributed control framework in DC microgrids," *IEEE Transactions on Smart Grid,* vol. 12, no. 1, pp. 205-214, 2020.

[16] Z. Hossain, S. Ahmad, U. K. Jhuma, S. Mekhilef, M. Mubin, H. Mokhlis, and T. Ahmed, "A Flexible Interconnection and Power Sharing Strategy For Two Autonomous Microgrid Systems," in *2021 IEEE 6th International Conference on Computing, Communication and Automation (ICCCA)*, 2021, pp. 472-477: IEEE.

[17] D. Saha, N. Bazmohammadi, J. C. Vasquez, and J. M. Guerrero, "Multiple microgrids: A review of architectures and operation and control strategies," *Energies,* vol. 16, no. 2, p. 600, 2023.

[18] L. Fan and Z. Miao, "Mitigating SSR using DFIG-based wind generation," *IEEE Transactions on Sustainable Energy,* vol. 3, no. 3, pp. 349-358, 2012.

[19] M. N. Tasnim, T. Ahmed, M. A. Dorothi, S. Ahmad, G. Shafiullah, S. Ferdous, and S. Mekhilef, "Voltage-Oriented Control-Based Three-Phase, Three-Leg Bidirectional AC–DC Converter with Improved Power Quality for Microgrids," *Energies,* vol. 16, no. 17, p. 6188, 2023.

[20] M. Parvez, M. F. M. Elias, N. Abd Rahim, F. Blaabjerg, D. Abbott, and S. F. Al-Sarawi, "Comparative study of discrete PI and PR controls for single-phase UPS inverter," *IEEE Access,* vol. 8, pp. 45584-45595, 2020.

2023 10th IEEE International Conference on Power Systems (ICPS)
13-15 December 2023, Cox's Bazar, Bangladesh

Performance of Microgrid Systems on Multiple Dynamic Loads Penetration

Tajrin Jahan Rumky[1,2], Tofael Ahmed[3], Moudud Ahmed[4], Shameem Ahmad[5], and M. M. Rahman [6]
[1,3]*Advanced Power System Laboratory, Department of Electrical & Electronic Engineering, Chittagong University of Engineering and Technology (CUET), Chittagong 4349, Bangladesh.*
[2]*Department of Electrical and Electronic Engineering, Southern University Bangladesh,* Chattogram, Bangladesh
[3]*Department of Electrical and Electronic Engineering, Bangabandhu Sheikh Mujibur Rahman Science and Technology University, Gopalganj -8100, Bangladesh.*
[4]*Department of Electrical & Electronic Engineering, Faculty of Engineering, American International University - Bangladesh (AIUB), Dhaka 1229, Bangladesh.*
[5]*Department of Electrical and Electronic Engineering, East Delta University, Chattogram, Bangladesh*
Email- tajrinrumky16@gmail.com, tofael@cuet.ac.bd, moudud.eee@gmail.com, ahmad.shameem@aiub.edu, mahbubur.r@eastdelta.edu.bd

***Abstract*—Microgrids (MGs) have emerged as a promising solution to enhance the reliability and sustainability of modern power distribution systems. In recent years, there has been a growing interest in interconnecting multiple microgrids to create more resilient and efficient energy networks. However, the performance of interconnected microgrids under various dynamic load scenarios remains a critical research area. In this paper, problems like low-frequency oscillations (LFOs) and the dynamic performance of multiple induction motors (IMs) in microgrids instead of a single motor with the same rating under a wide range of operating conditions are looked at. A single microgrid and an interconnected microgrid are two alternative model configurations designed in Matlab/Simulink that are considered in this study's comparison of non-linear dynamic simulations. The findings show that, compared to a local microgrid system, the performance of an interconnected microgrid system is more susceptible to being impacted by several parallel IM loads. Furthermore, it has been discovered that large IMs have lower LFO damping capabilities than parallel multiple small IMs.**

Keywords—dynamic loads, interconnected microgrid, local microgrid, induction motor (IM), low-frequency oscillations (LFOs).

I. INTRODUCTION

Microgrids are small-scale, localized energy systems that can operate independently or in conjunction with the main grid. They are characterized by their ability to integrate various distributed energy resources, including renewable sources, energy storage systems, conventional generators, and multiple types of loads [1]. This microgrid can be represented as a local microgrid. The dynamic performance and stability of microgrids are essential for ensuring a reliable and resilient power supply. Advanced control, security, and communication technologies are essential for the successful expansion of a microgrid framework because they guarantee superior power quality, effective power management, balance in power distribution, and intelligent monitoring [2]. One approach to further improving the performance and reliability of microgrids is to interconnect them with another microgrid system to form a larger network [3]. Interconnected microgrids can share resources, increase overall system stability, and provide better support for loads. Moreover, the integration of microgrids has a profound impact on various aspects of the network, including power quality, voltage, and frequency control, which significantly influence the dynamic stability of the system within acceptable limits when subjected to disturbances [4, 5].

Since electrical loads are the main component of a power system, the effect of dynamic stability on microgrids can differ depending on the types of loads connected to the microgrid [6]. Induction motors (IMs) are so widespread in industry that they account for more than 30% of the world's total energy usage [7, 8]. Managing induction motor loads, which can have a significant impact on system stability and performance, is one of the key issues in the successful implementation of microgrids, alongside other loads such as constant impedance, constant current, and constant power [9]. Moreover, the dynamic characteristics of induction motor loads can introduce challenges related to voltage dips, frequency variations, harmonic distortions, and control requirements in overall microgrid operation. It would be impractical to analyze a local or interconnected microgrid without taking IM dynamics into account due to their non-linear dynamics and the fact that both large and small IMs are usually directly connected to low- or medium-voltage distribution networks. In an induction motor, an air gap between the rotor and stator generates an electromagnetic field that forces the rotor to turn. In normal, steady-state operation, the electrical torque produced by the interaction of the electromagnetic field with the rotor is equal to the mechanical torque required to turn the load, ensuring a constant rotor speed and smooth motor operation. However, sudden changes or disturbances can disrupt this balance, leading to low-frequency oscillations (LFOs) in the rotor speed, as IM's rotor speed oscillations are directly coupled with the system frequency. These LFOs can affect the microgrid system in multi-oscillatory modes. To stabilize the local and interconnected microgrid system in the presence of IM loads, a tri-band damping controller is proposed for sustaining transient

979-8-3503-1873-9/23/$31.00

sustaining transient disturbances [10]. The rotor time constant is another significant IM component, which depends on rotor resistance, rotor resistance, and mutual inductance and increases when machine power rating rises. The rotor-circuit time constant is relatively low for small IMs compared to large IMs with the same power rating, resulting in a fast decay of rotor electro-mechanical dynamics [11]. Therefore, it is necessary to investigate the performance of a microgrid system under multiple small IMs and a large IM with the same power rating.

Microgrids are expected to become more prevalent in future power networks due to their high penetration and advancements in power converter ratings and topologies. Interconnected microgrid systems will be subjected to a wide range of static and dynamic loads where electromechanical rotor oscillation phenomena occur due to the highly nonlinear load dynamics, as large IM loads can interact with synchronous generator rotor dynamics and excitation systems, leading to modal resonances, limit cycles, and voltage oscillations [12]. Therefore, it is crucial to consider the non-linear dynamic behaviors of large IMs while studying the stability of an interconnected microgrid system.

This paper focuses on assessing the impact of multiple dynamic loads on the performance of a local microgrid system and an interconnected microgrid system. To better understand these effects, we compare the performance of microgrids under multiple dynamic loads to that under single dynamic loads with equivalent ratings in Matlab/Simulink.

The remainder of this document is structured as follows: In Sections II and III, we provide concise discussions on the simulation platform and modelling of IM (induction motor) respectively. Section IV presents the induction motor's torque-speed characteristics and variations. Section V briefly explains the non-linear dynamic simulation results. Finally, in Section VII, we summarize the conclusions drawn from this study and provide a brief overview.

II. Description of the Simulation Platform

A. Local Microgrid System

The local microgrid system is made up of several components, including two photovoltaic (PV) systems, one energy storage system (ESS), a diesel generator, a wind generator, constant impedance loads, and induction motor loads in fig.1. This system has a power generation capacity of 900 kW, operates at a 400 V AC bus voltage, and has a frequency of 50 Hz. To deal with the variability in power

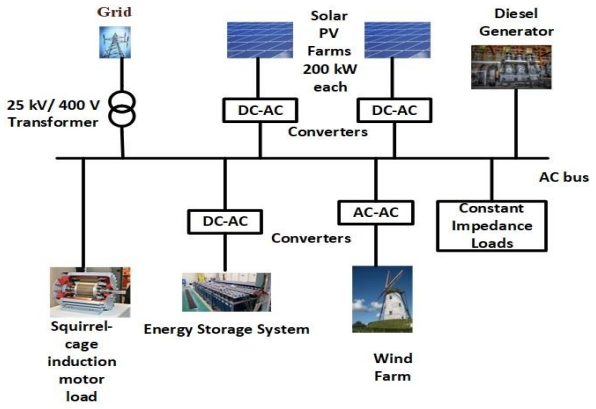

Fig.1. Schematic diagram of local microgrid system.

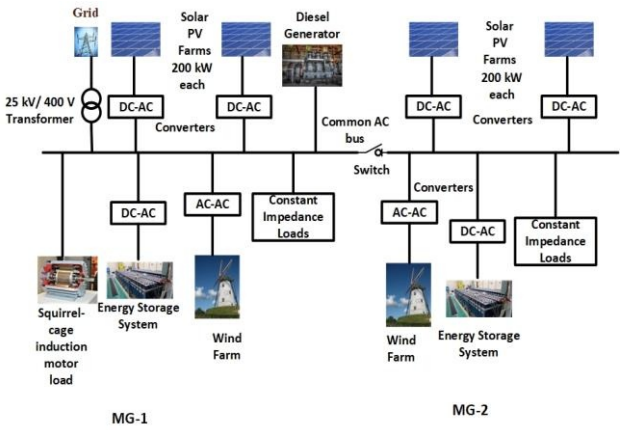

Fig.2. Schematic diagram of interconnected microgrid system

generation from renewable sources like wind and solar, a 200 kVA ESS is connected to the AC bus to provide backup power when needed. Both the ESS and the diesel generator are used as backup power sources to counter the unpredictable nature of wind and solar energy. This microgrid comprises two PV farms generating 200 kW each, a 350 kW wind generator, and a 150 kW diesel generator. The system is linked to the distribution feeder through a 25 kV/400 kV distribution transformer at the point of common coupling (PCC).

B. Interconnected Microgrid System

The interconnected microgrid system comprises two parts: MG-1 and MG-2, as depicted in fig. 2. MG-2 is designed as another local microgrid system with two PV systems of 200 kW each, a 350 kW wind farm, a 200 kVA energy storage system, and constant impedance loads. Both microgrids share a common AC bus but are connected through a static switch. They each maintain their own unique configurations. The combined installed capacity of the interconnected microgrid system is 1650 kW. There are individual voltage source converters (VSCs) for each distributed generation and an ESS with a damping control architecture in each microgrid [10]. Frequency measurement employs a phase-locked loop.

III. Mathematical Modelling of an Induction Motor

A fourth-order state-space model of the machine's electrical component and a second-order system of the machine's mechanical component are used to depict them. The arbitrary two-axis *dq* reference frame is used for all stator and rotor quantities. The fundamental voltage equations of an induction motor in a stationary dq reference frame are given in terms of currents and fluxes for both stator and rotor [13] in equations 1-4:

$$v_{qs} = R_s i_{qs} + \frac{d\varphi_{qs}}{dt} + \omega\varphi_{qs} \quad (1)$$

$$v_{ds} = R_s i_{ds} + \frac{d\varphi_{ds}}{dt} - \omega\varphi_{qs} \quad (2)$$

$$v_{qr} = R_r i_{qr} + \frac{d\varphi_{qr}}{dt} + (\omega - \omega_r)\varphi_{dr} \quad (3)$$

$$v_{dr} = R_r i_{dr} + \frac{d\varphi_{dr}}{dt} - (\omega - \omega_r)\varphi_{qr} \quad (4)$$

Here, the reference frame angular velocity and electrical angular velocity are denoted by ω, ω_r respectively. R_r, R_s are rotor and stator resistance, respectively, while the subscripts r and s stand for rotor and stator quantities, respectively. In equation 5, T_e denotes the electromagnetic torque expressed in terms of stator fluxes and currents, where p is the number of poles of the induction motor.

$$T_e = \frac{3}{2}\, p\, (\varphi_{ds}\, i_{qs} - \varphi_{qs}\, i_{ds}) \quad (5)$$

The flux linkages of an induction motor are represented by the parameter φ, with suitable subscripts mentioning the reference frame axis with rotor and stator, and the equations can be expressed by equations 6-11 [14]:

$$\varphi_{qs} = L_s i_{qs} + L_m i_{qr} \quad (6)$$

$$\varphi_{ds} = L_s i_{ds} + L_m i_{dr} \quad (7)$$

$$\varphi_{qr} = L_r i_{qr} + L_m i_{qs} \quad (8)$$

$$\varphi_{dr} = L_r i_{qr} + L_m i_{ds} \quad (9)$$

$$L_r = L_{lir} + L_m \quad (10)$$

$$L_s = L_{lis} + L_m \quad (11)$$

Where L stands for an induction motor's inductances with the appropriate subscripts. While the subscripts *lis* and *lir* denote the leakage inductance of the stator and rotor, respectively, the subscripts *m*, *r*, and *s* denote the magnetizing components, rotor, and stator, respectively.

The torque created when electrical power is transformed inside a machine into mechanical power is referred to as induced torque. This torque is countered by the torques created by friction and wind resistance within the machine; thus, it differs from the torque that can be measured at the motor's terminals [15]. The following is the formula for determining the induced torque, τ_{ind}:

$$\tau_{ind} = \frac{P_{conv}}{\omega_m} = \frac{P_{ag}}{\omega_{sync}} = \frac{3\, V_{th}^2\, {R_r}/{s}}{\omega_{sync}\left[\left(R_{th} + {R_r}/{s}\right)^2 + \left(R_{th} + {R_r}/{s}\right)^2\right]} \quad (12)$$

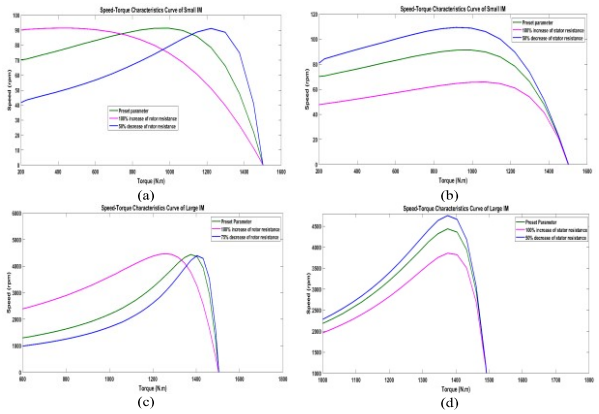

Fig. 3. Torque-speed characteristics curves, (a) for small IM with deviation of rotor resistance from preset values, (b) for small IM with deviation of stator resistance from preset values, (c) for large IM with deviation of rotor resistance from preset values, and (d) for large IM with deviation of stator resistance from preset values.

Where P_{conv} is converted to power in mechanical form in an induction motor, P_{ag} represents air-gap power; s denotes slip of the rotor, ω_m and ω_{sync} denote rotor speed and synchronous speed, respectively; and subscripts th denote the thevenin equivalent quantity.

IV. Induction Motor Torque-Speed Characteristic Variations

For both small and large IMs, a torque-speed characteristics curve will be drawn. By altering the default IM parameters, comparison research will be conducted using the torque-speed characteristics curve. Fig. 3 (a) and (b) indicate the torque-speed characteristics for a small IM (5.4 hp IM) for a change in rotor resistance (Rr) and stator resistance (Rs), while Fig. 3 (c) and (d) indicate the torque-speed characteristics for a large IM (215 hp IM). For both forms of IM, it can be seen that torque fluctuates as rotor resistance deviates from set levels. Initial torque is higher when rotor resistance is raised than when it is decreased as the positive primary factor. When the stator resistance changes, however, the situation reverses as a negative secondary factor.

V. Simulation Results

The performance of the two microgrid systems was evaluated considering LFO characteristics using nonlinear dynamic simulations that considered small and large IM loading patterns with equal power ratings as well as disturbances in the microgrid systems.

The simulation and analysis were done while comparing the dynamic performance of 40 parallel 5.4-hp (4 kW) IMs and a 215-hp (160 kW) large IM at the different microgrid systems. The following scenarios are considered for dynamic simulation studies and analysis:

A. Case 1: Local microgrid system taking into consideration 15.09% of IM loading patterns under 37.74% of load disturbances for several small IMs and a large IM separately

In this case study, the local microgrid system has been considered among the two types of microgrid configurations stated before. The local microgrid has a 900-kW total generation capacity and is operating at 73.33% loading (with a 500-kW constant impedance load and a 160-kW IM load). At t=2s, a 400-kW step load is added to cause the disturbances. At t=3s, the load is withdrawn, and the performances of the microgrid system are recorded for further analysis. AC microgrid system's point of common coupling (PCC) voltage and frequency are illustrated in fig. 4 (a) & (b) respectively. Furthermore, when a 400-kW step load is introduced into the microgrid, single IMs loading exhibits a maximum frequency deviation of 49.89 Hz whereas, 49.86 Hz frequency deviation holds for multiple small IMs loading condition. With the increase in IM loading numbers within equal power ratings, 4 volts of system voltage are fluctuating during the starting of the motor. The voltage and frequency oscillations in the microgrid system are caused by load disturbances. Voltage and frequency fluctuations within the microgrid can lead to rotor speed oscillations for several reasons. Firstly, the power consumption of induction motors (IMs), including both active and reactive power, is affected by variations in the stator voltage and rotor speed. Secondly, fluctuations in

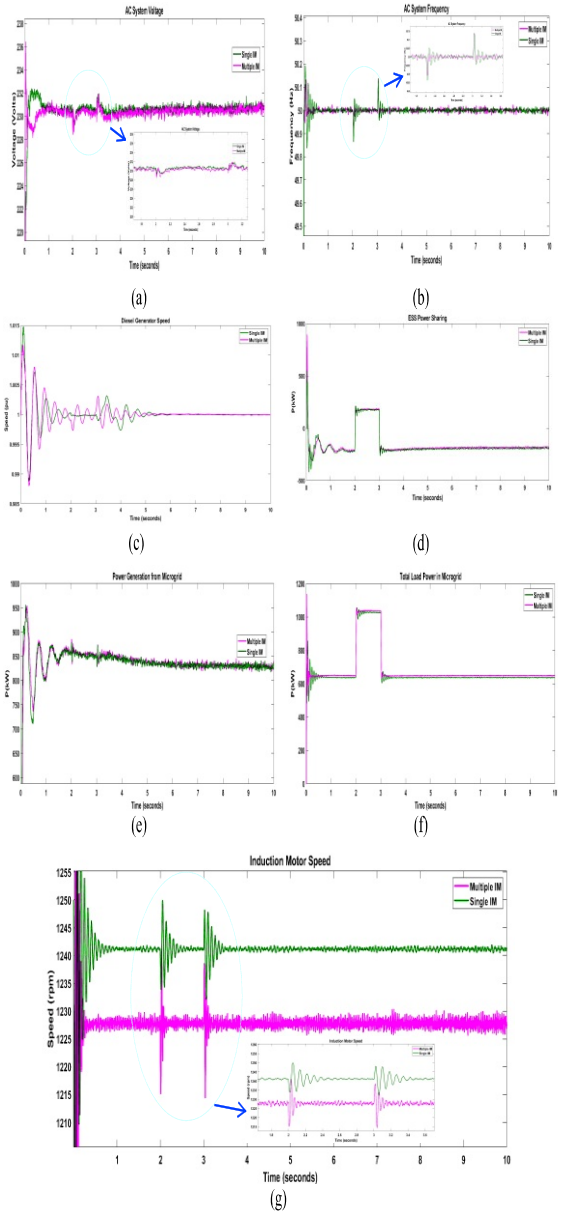

Fig. 4. Local microgrid system with 15.09% of IM loading patterns under 37.74% of load disturbances for both several small IMs and a large IM condition, (a) AC system voltage, (b) AC system frequency, (c) Diesel generator speed, (d) ESS power sharing, (e) Power generation from microgrid, (f) Total load curve in microgrid, and (g) Induction motor speed.

frequency directly induce oscillations in the rotor speed of induction motors. Lastly, alterations in rotor speed can, in turn, impact power consumption which is seen in fig. 4 (f) at time t=2s when a step load of 400-kW is injected into the system. The ESS's output power in fig. 4 (d) indicates that when a step load is introduced, it supplies approximately 71 kW of active power for a single large IM, whereas it provides only 41 kW of active power for multiple smaller IMs. Diesel generators are typically rated to handle brief overloads, but if the combined inrush current of all the motors exceeds the generator's capacity, it can lead to a speed deviation which is visible in fig. 4 (c). For a single large IM, the diesel generator speed deviation is lower than the multiple small IMs. As a result, a type of LFOs introduced in [10], is getting more severe for multiple small IMs in a local microgrid system.

B. *Case 2: Interconnected microgrid system taking account of both several parallel small IMs and a large IM penetration separately, with 15.09% of IM loading under 37.74% of load disturbances in MG-1 and 53.33% of loading condition under 26.32% of load disturbances in MG-2*

In this scenario, an interconnected microgrid has been considered where a local microgrid system (MG-1) is integrated with another microgrid (MG-2), which falls into the microgrid configuration previously mentioned in fig. 5. The system has a total generation capacity of 1650 kW and is currently working at 64.24% capacity. The installed capacity of the MG-1 is 900 kW, and it is operated at 73.33%% loading (500 kW as a constant impedance load

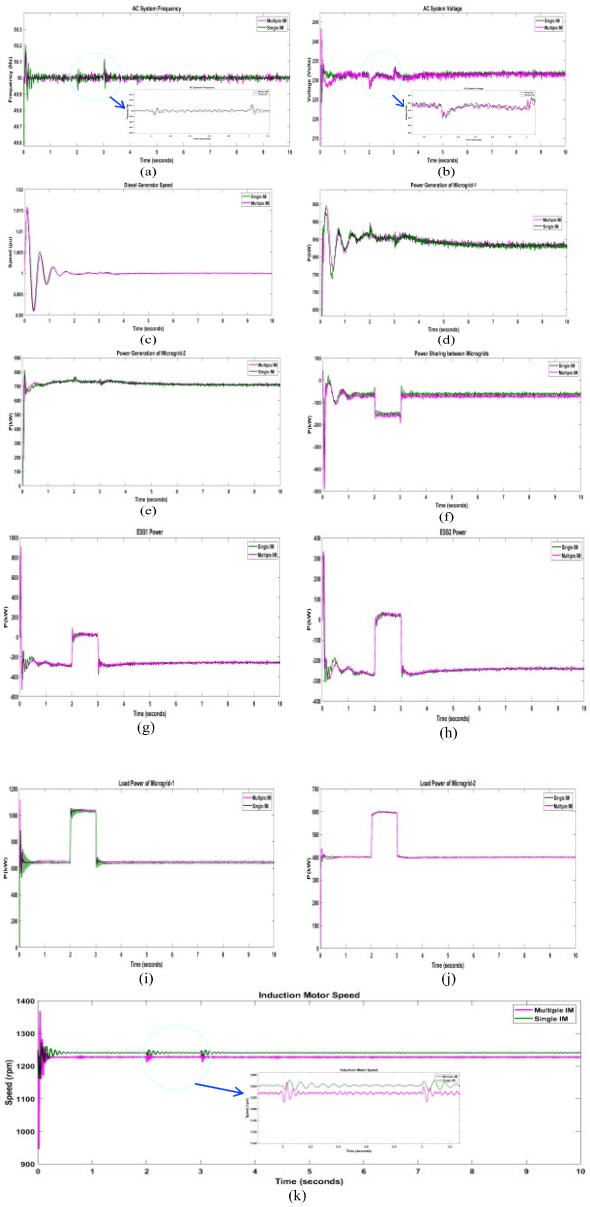

Fig. 5. An interconnected microgrid system with 15.09% of IM loading under 37.74% of load disturbances in MG-1 and 53.33% of loading condition under 26.32% of load disturbances in MG-2 for both several small IMs and a large IM condition, (a) AC system frequency, (b) AC system voltage, (c) Diesel generator speed, (d)Power generation of MG-1, (e) Power generation of MG-2, (f) Power sharing between microgrids, (g) ESS power of MG-1, (h) ESS power of MG-2, (i) Load power of MG-1, (j) Load power of MG-2, and (k) Induction motor speed.

and a 215 hp IM). The total generation capacity of the MG-2 is 750 kW, and it is operated at 53.33% load with only a 400 kW constant impedance load. At t = 2s, a 400 kW step load is added in MG-1 and a 200 kW step load in MG-2 to cause disturbances, and at t = 3s, these loads are removed to examine the functioning of the microgrid in more detail.

When the extra 200 kW constant impedance load is linked to the MG-2, it draws power from the MG-2. This decrease in power supplied from the MG-2 to the MG-1 causes a shortage of power in the MG-1. To compensate for this power imbalance, the ESS connected to the point of common coupling in the MG-1 is utilized, as shown in fig. 5 (d-j). As a result of this sudden change in load, the voltage of the common AC bus of the interconnected system starts to fluctuate as illustrated in fig 5 (b), leading to oscillations in the speed of the IM rotor in fig 5 (k). The rotor speed settled after about the sixth peak in the single IM case, but after the third peak in the multiple IM case and the settled duration is shorter in this case for this configuration of microgrid system. Additionally, when step loads are introduced in both microgrids, it is seen in fig 5 (a) that the single IMs experience a comparatively smaller frequency deviation than multiple small IMs.

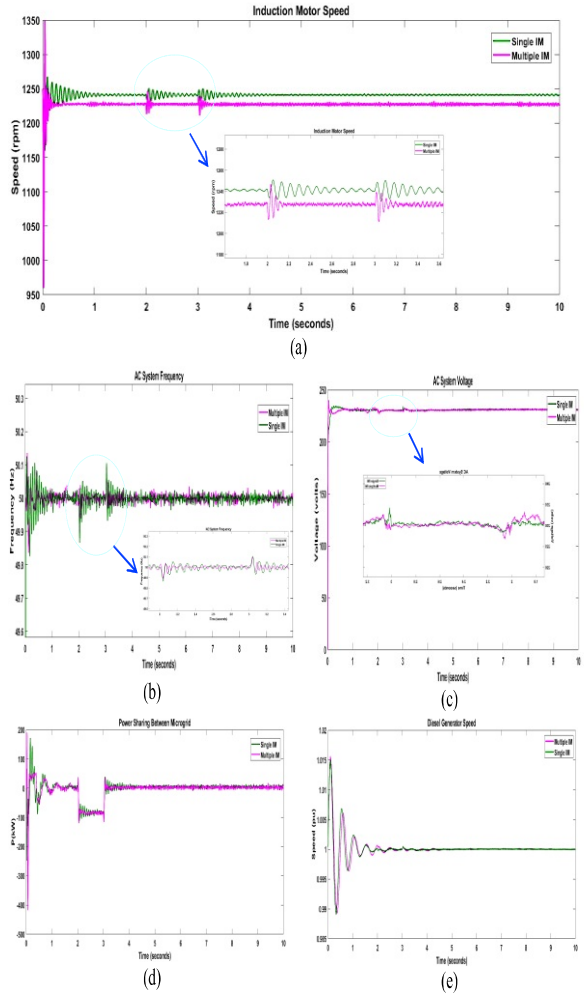

Fig. 6. An interconnected microgrid system with 15.09% of IM loading under 37.74% of load disturbances in MG-1 and 21.05% IM loading under 26.32% of load disturbances in MG-2 for both several small IMs and a large IM condition, (a) Induction motor speed, (b) AC system frequency, (c) PCC voltage, (d) Power sharing between microgrids, and (e) Diesel generator speed.

C. Test mode 1: Interconnected microgrid system taking account of several parallel small IMs and a large IM penetration separately, with 15.09% of IM loading under 37.74% of load disturbances in MG-1 and 21.05% of IM loading under 26.32% of load disturbances in MG-2

In this part, IM loading in both microgrids is introduced to better understand the dynamic behavior of both forms of IM. It is significant to notice that although the scenario has been applied with a comparable load disturbance to prior case 2 for both microgrids, the IM loading for both microgrids has altered due to the changed loading level. As can be seen, MG-1 operates with 15.09% of IM loading while experiencing 37.74% load disturbances, whereas MG-2 operates with 21.05% of IM loading while experiencing 26.32% load disturbances. The IM rotor speed and the system frequency are depicted in fig. 6 (a) and (b), respectively. Additionally, fig. 6 (c) and (d) show, respectively, the PCC voltage and the power sharing between microgrids. It is found that having numerous parallel working IMs increases non-linearity in the system dynamics. Furthermore, increasing dynamic loads (i.e., IMs) causes greater rotor speed oscillations and frequency deviations in the interconnected microgrid, necessitating higher damping torque. But the diesel generator's speed oscillation settle time is reduced by 0.2 seconds when a single IM is installed instead of the many IMs shown in fig. 6 (e).

D. Test mode 2: Interconnected microgrid system taking account of both several parallel small IMs and a large IM penetration in MG-1 with 22.22% of each type of IM loading under 32.78% of load disturbances and 33.33% multiple parallel IM load penetration under 26.32% of load disturbances in MG-2

In this test scenario, MG-1 is subjected to both forms of IM loading, whereas MG-2 is subjected to multiple small IM loading categories. Fig. 7 (a) and (b) illustrate the rotor speeds of the small and big IMs with and without disturbances when both types of IMs are coupled in MG-1. Small IM exhibits a 30% greater speed deviation than without interruptions, but large IM shows a 25% greater speed deviation. As a result, it is revealed that multiple parallel operating IMs show more non-linearity than a large IM.

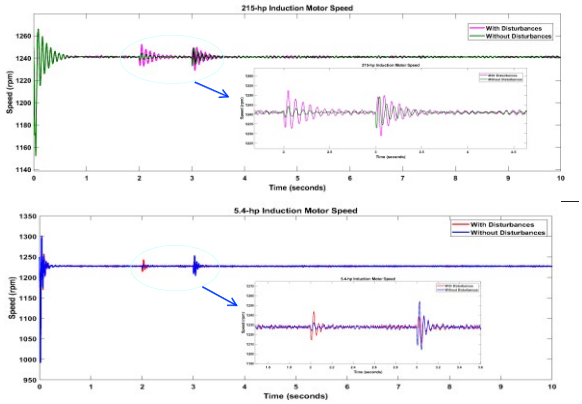

Fig. 7. Induction motor speed of MG-1 with and without disturbances, (a) Rotor speed of multiple small IM and (b) Rotor speed of large IM.

VI. Conclusions

This research delved into the dynamic effects of introducing both small and large induction motor loads in microgrids. The findings of this study underscore the significant influence of IM model parameters, with rotor resistance emerging as the positive primary factor and stator resistance emerging as the negative secondary factor affecting its dynamic performance. Additionally, non-linear dynamic simulations of a large single induction motor or several small parallel induction motors with sudden load changes for two microgrid configurations are used to examine the dynamic performance of IMs. It is obvious that the sudden load fluctuations have a major impact on the IM rotor speed, system frequency, and power sharing from energy storage systems.

- **IM Rotor Speed**: Rapid load changes in induction motors can cause significant rotor speed variations, posing challenges in managing these variations, particularly in systems with multiple motors.
- **System Frequency**: The frequency of the microgrid system is directly influenced by fluctuations in the load. As induction motors are sensitive to changes in frequency, sudden load changes can lead to frequency deviations. This can have a cascading effect on the overall stability and performance of the microgrid.
- **Power Sharing from Energy Storage Systems (ESS)**: The study reveals that load fluctuations affect power distribution from energy storage systems (ESS), which are crucial for microgrid supply and demand balance, affecting their efficiency and lifespan.

Appendix

5.4-hp (4 kW) IM parameters:
R_r = 1.395 Ω, R_s = 1.405 Ω, H = 0.0131 kgm^2, L_r = 0.005839 H, L_s = 0.005839 H, P = 2, and L_m = 0.00769 H.
215-hp (160 kW) IM parameters:
R_r = 0.007728 Ω, R_s = 0.01379 Ω, H = 2.9 kgm^2, L_r = 0.000152 H, L_s = 0.000152 H, P = 2, and L_m = 0.00769 H.
The specifications for the distributed generations and ESS control of the microgrids are derived from study [10].
Parameters of the damping controller:
Global gain=1.0, Low frequency band (FL(Hz), KL) = 0.2, 30, Intermediate frequency band (FI(Hz), KI) = 1.25, 40, High frequency band (FH(Hz), KH) = 12.0, 160, Signals limits (VL_{max}, VI_{max}, VH_{max}, VS_{max}) = 0.075, 0.15, 0.15, 0.15, K_D = 160, and Wash-out filter time constant = 10s
PV Farms parameters:
Power = 200 kW, Parallel string = 88, Module per string = 7, Open-circuit voltage = 85.3V, Short-circuit current = 6.09A, Voltage at MPPT = 72.9V, Current at MPPT = 5.69A
Diesel Generator parameters:
Power = 150kW, Pole pairs = 2, Inertia co-efficient, H = 3.2s, Friction factor = 0.08 pu, Rotor speed deviation = 0.05%, w_{ref} = 1.0 pu, Stator resistance, $R_s = 2.8544\times10^{-3}$ pu
ESS Parameters:
Power = 200kVA, Rated capacity = 700 Ah, Nominal voltage = 2000V, Initial state-of-charge (SoC) = 80%, Capacitance = 500μF, $L_1 = 6\times10^{-3}$ H, $L_2 = 5\times10^{-4}$ H, C = 5×10^{-5} F and R = 0.05 Ω, K_p = 10, K_i = 95, K_{pf} = 1, K_{if} = 50, K_{pv} = 0.5, K_{iv} = 1
DFIG Parameters:
Power = 350 kW, Rotor-type = Wound, Stator resistance, R_s = 0.023 pu, Stator inductance, L_{ls} = 0.18 pu, Rotor resistance, R_r = 0.016 pu, Rotor inductance, L_{lr} = 0.16 pu, Magnetizing inductance, L_m = 2.9 pu, Inertia constant, H = 0.685 s, Friction factor, F = 0.01 pu, and Pole pairs, p = 3

Acknowledgement

The authors thank the Chittagong University of Engineering and Technology (CUET) for providing financial support under the Development of CUET Project and Project No. CUET/DRE/2022-23/EEE/017.

References

[1] N. A. Hatziargyriou, Hiroshi & Iravani, Reza & Marnay, Chris, "Microgrids," *Power and Energy Magazine, IEEE,* vol. 5, pp. 78-94, 2007, doi: 10.1109/MPAE.2007.376583.

[2] M. N. Tasnim, T. Ahmed, S. Ahmad, and S. Mekhilef, "Hardware in The Loop Implementation of The Control Strategies for The AC-Microgrid in OPAL-RT Simulator," in *2023 IEEE IAS Global Conference on Renewable Energy and Hydrogen Technologies (GlobConHT)*, 2023: IEEE, pp. 1-6.

[3] Z. X. a. P. Y. a. C. Z. a. Y. Z. a. J. P. a. Z. Zeng, "Analysis on the organization and Development of multi-microgrids," *Renewable and Sustainable Energy Reviews,* vol. 81, pp. 2204-2216, 2017, doi: https://doi.org/10.1016/j.rser.2017.06.032.

[4] Z. Shuai, Y. Peng, X. Liu, Z. Li, J. M. Guerrero, and Z. J. Shen, "Dynamic equivalent modeling for multi-microgrid based on structure preservation method," *IEEE Transactions on Smart Grid,* vol. 10, no. 4, pp. 3929-3942, 2018.

[5] N. Roy, H. Pota, M. Mahmud, and M. Hossain, "Voltage control of emerging distribution systems with induction motor loads using robust LQG approach," *International Transactions on Electrical Energy Systems,* vol. 24, no. 7, pp. 927-943, 2014.

[6] R. Majumder, "Some aspects of stability in microgrids," *IEEE Transactions on power systems,* vol. 28, no. 3, pp. 3243-3252, 2013.

[7] F. J. Ferreira and A. T. de Almeida, "Overview on energy saving opportunities in electric motor driven systems-Part 2: Regeneration and output power reduction," in *2016 IEEE/IAS 52nd Industrial and Commercial Power Systems Technical Conference (I&CPS)*, 2016: IEEE, pp. 1-8.

[8] M. Ahmed, A. Vahidnia, L. Meegahapola, and M. Datta, "Impact of multiple motor loads on dynamic performance and stability of microgrids," in *2019 IEEE International Conference on Industrial Technology (ICIT)*, 2019: IEEE, pp. 1704-1709.

[9] J. V. Milanovic, S. C. Vegunta, and M. T. Aung, "The influence of induction motors on voltage sag propagation—Part II: Accounting for the change in sag performance at LV buses," *IEEE transactions on power delivery,* vol. 23, no. 2, pp. 1072-1078, 2008.

[10] T. J. Rumky, T. Ahmed, M. Ahmed, and S. Mekhilef, "Tri-Band Damping Controller for Low Frequency Oscillations in AC Microgrid System," in *2023 IEEE IAS Global Conference on Renewable Energy and Hydrogen Technologies (GlobConHT)*, 2023: IEEE, pp. 1-6.

[11] J. J. Cathey, R. K. Cavin, A. Ayoub, and Systems, "Transient load model of an induction motor," *IEEE Transactions on Power Apparatus and Systems,* no. 4, pp. 1399-1406, 1973.

[12] M. Naderi, Y. Khayat, Q. Shafiee, F. Blaabjerg, and H. Bevrani, "Dynamic modeling, stability analysis and control of interconnected microgrids: A review," *Applied Energy,* vol. 334, p. 120647, 2023.

[13] P. W. P. Dattaray, V. Terzija, D. Chakravorty, P. Mohapatra and J. Yu, "Impact of load dynamics on torsional interactions," presented at the Power Systems Computation Conference (PSCC), Genoa, Italy, 2016.

[14] J. J. Cathey, *TRANSIENT-LOAD MODEL OF AN INDUCTION MOTOR*. Texas A&M University, 1972.

[15] N. Afrin, F. Yang, J. Lu, and M. Islam, "Impact of induction motor load on the dynamic voltage stability of microgrid," in *2018 Australian & New Zealand Control Conference (ANZCC)*, 2018: IEEE, pp. 397-402.